DESIGN OF THE PIP-II TUNNEL GEODETIC CONTROL NETWORK

D. P. Krawczuk†, Fermi National Accelerator Laboratory, Batavia, IL, USA

Abstract

Fermilab's PIP-II project will result in a new beamline approximately 550 meters long. A geodetic control network will need to be established to precisely align the beamline components in the tunnel. This design focused on the tunnel network, as the surface network had already been considered. After selecting the geometry, instrumentation, and methodology, a pre-analysis was performed to estimate the global network uncertainties. Local errors were also estimated by considering alignment procedures and instrument noise. The global and local errors were then combined to estimate the total alignment uncertainty, which was compared against the project's alignment accuracy requirements.

INTRODUCTION

The purpose of the Proton Improvement Plan-II (PIP-II) project is to build a new superconducting radiofrequency (SRF) linear accelerator (Linac) that will generate a high-energy particle beam that will be used for various physics experiments at Fermilab, including the new Deep Underground Neutrino Experiment (DUNE) at the Long Baseline Neutrino Facility (LBNF). Starting from the ion source in the warm front-end, H-minus ions will be accelerated to 2.1 MeV energy levels via a radio-frequency quadrupole (RFQ). They will then enter the 215-meter long Linac in the superconducting section where they will be accelerated to 800 MeV energy levels. The H-minus ions will then be transported to Fermilab's existing Booster Ring through the Beam Transfer Line (BTL) and will then be injected into the Booster Ring [1]. All beamline components will be placed in an underground tunnel that consists of a straight section and a curved section (see Fig. 1). The straight section will contain both the warm front-end and the Linac, and the curved section will contain the BTL, giving a total beam length of approximately 550 meters.

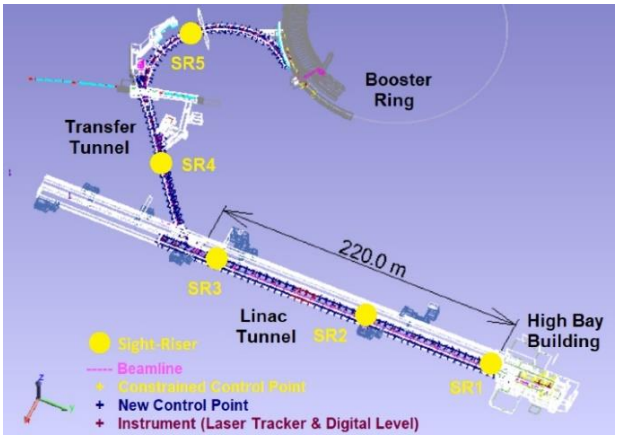

Figure 1: Overall View.

† krawczuk@fnal.gov

TOLERANCE REQUIREMENTS

There are three main tolerance requirements that are outlined in the PIP-II Alignment Network Technical Requirements Specification [2] and PIP-II Misalignment Tolerances Physics Requirement Document (the values in the tables are shown to a 1σ confidence level) [3]. Note that all uncertainty requirements and results are shown to a 1σ confidence level for the entirety of this document.

The PIP-II project utilizes two geodetic coordinate systems, and both are called the "Fermi Site Coordinate System (FSCS)". The first system, FSCS-H, is defined by a double stereographic projection and heights above the DUSAF datum and is used for survey purposes. The second system, FSCS-Z, is defined by a plane that is tangent to the ellipsoid at a point close to the middle of the site and is used for lattice design purposes [4]. Fermilab's Alignment and Metrology Department (AMD) uses the "Lattice" program (University College London, London, England) to convert between all site coordinate systems, including FSCS-H and FSCZ-Z [5]. The following two tolerance requirements are with respect to the FSCS-Z system:

1. The Alignment Network shall provide a single-point absolute measurement accuracy of 0.50 mm.
2. The Alignment Network shall provide a relative measurement accuracy of 0.25 mm between points separated by less than 100 meters.

Multiparticle simulations of the beam dynamics were run to estimate individual component alignment tolerances. The simulations focused on being able to propagate the particle beam through the whole SRF Linac (approximately 175 meters long) with a high probability and without orbit correction [6]. This means that the provided alignment tolerances are relative to a best-fit line that is 175 meters long; they are not component-to-component tolerances. This requirement was extended to include the entire 550-meter-long beamline for network verification purposes. The third tolerance requirement can therefore be stated in the following way:

3. The component misalignments must satisfy the requirements in Tables 1 – 3. The misalignments are expressed in terms of shifts (longitudinal, transverse, and elevation) and orientations (pitch, roll, and yaw) with respect to the ideal beamline position in the FSCS-Z system.

GEODETIC CONTROL NETWORK (GCN) DESIGN

Figure 1 shows the tunnel geometry and the proposed methodology. The GCN consists of the surface network (SN) and the tunnel network (TN). The SN has already

Table 1: Cold Component Alignment Tolerances

Beamline Element	Transverse (mm)	Vertical (mm)	Longitudinal (mm)	Pitch (mrad)	Yaw (mrad)	Roll (mrad)
NR = No Requirements, F = Fulfilled by Meeting Transverse/Vertical Requirements						
Cavities						
HWR Cavity	0.5	0.5	1	3	3	NR
SSR1 Cavity	0.5	0.5	1	3	3	NR
SSR2 Cavity	0.5	0.5	1	3	3	NR
LB650 Cavity	0.5	0.5	1	2	2	NR
HB650 Cavity	0.5	0.5	1	1	1	NR
Solenoids						
Solenoid HWR	0.5	0.5	1	1	1	5
Solenoid SSR1	0.5	0.5	1	1	1	5
Solenoid SSR2	0.5	0.5	1	1	1	5
Cold Instrumentation						
Cold BPMs	0.5	0.5	1	F	F	5

Table 2: Warm Component Alignment Tolerances

Beamline Element	Transverse (mm)	Vertical (mm)	Longitudinal (mm)	Pitch (mrad)	Yaw (mrad)	Roll (mrad)
NR = No Requirements, F = Fulfilled by Meeting Transverse/Vertical Requirements						
Front End						
Ion Source	0.25	0.25	5	F	F	NR
LEBT Solenoid	0.25	0.25	5	F	F	40
LEBT Dipole Magnet	0.25	0.25	5	F	F	F
LEBT Chopper	0.25	0.25	5	F	F	NR
RFQ Entrance/Exit	0.125	0.125	2	F	F	1
MEBT Quad	0.25	0.25	0.5	F	F	4
MEBT Corrector	1	1	0.5	F	F	4
Bunching Cavities	0.175	0.175	1	F	F	NR
200 Ohm Kicker	0.25	0.050	0.25	F	F	F
MEBT Absorber	1	0.125	1.5	0.25	2	5
Differential Pumping Insert	0.25	0.25	5	1	1	NR
SRF Linac						
RT Linac Quad	0.25	0.25	0.5	F	F	3
RT Steering Dipole	1	1	1	10	F	5
Straight Ahead Dump	1	1	5	5	5	NR

Table 3: Warm Component Alignment Tolerances (Continued)

Beamline Element	Transverse (mm)	Vertical (mm)	Longitudinal (mm)	Pitch (mrad)	Yaw (mrad)	Roll (mrad)
NR = No Requirements, F = Fulfilled by Meeting Transverse/Vertical Requirements						
BTL						
RT BTL Quad	0.25	0.25	0.5	F	F	3
RT BTL Dipole	0.25	0.25	0.5	F	F	2
RT Steering Dipole	1	1	1	10	F	5
BTL Septum	0.25	0.25	0.5	F	F	3
BTL Switch Dipole	0.25	0.25	0.5	F	F	3
BTL Beam Absorber	1	1	5	5	5	NR
Warm Instrumentation						
Faraday Cup	0.5	0.5	0.5	NR	NR	NR
Fast Faraday Cup	0.5	0.5	0.5	3	3	NR
LEBT Allison Scanner	1	1	1	5	5	5
MEBT Allison Scanner	1	1	1	1	3	5
RT BPM	0.25	0.25	0.5	F	F	5
Laser Wire	0.25	0.25	0.25	F	F	5
Wire Scanner	0.5	0.5	0.5	F	F	5
Scraper	0.25	0.25	0.25	3	3	3
ACCT	0.5	0.5	0.5	NR	NR	NR
DCCT	0.5	0.5	0.5	NR	NR	NR
RWCM	0.5	0.5	0.5	NR	NR	NR
Longitudinal Pickup	0.5	0.5	0.5	NR	NR	NR

been designed by others in AMD and so will not be expanded upon in this report [7]; the pre-analysis results will be referred to, but the focus of this report will be on the TN. The purpose of the SN is to be able to locate the TN in FSCS-Z and to strengthen the geometry which would normally be poor in the tunnel along the transverse dimension. The following points from the SN will be constrained to accomplish this:

- Exactly 5 SN points will be transferred through evenly spaced sight-risers.
- Approximately 31 points in the High Bay Building (HBB) will be observed from the surface.
- Approximately 24 points will already be observed around the Booster connection before the commencement of this survey project.

Control Point Placement and Instrumentation

The instruments used in this pre-analysis are shown in Table 4. The uncertainties for the laser tracker and digital level are based on results from previous tunnel network adjustments. AMD has only recently acquired the Leica TS60 total station; the manufacturer's specifications were used for the pre-analysis since the group did not yet have a chance to use this instrument in a network adjustment and determine experimental uncertainties.

Table 4: Chosen Instrument Uncertainties

Type	Model	Uncertainty
Laser Tracker	Leica AT40x	$\sigma_{Hz,V}$ = 1" σ_a = 0.008 mm σ_b = 2.5 ppm
Digital Level	Leica DNA03	σ_a = 0.050 mm σ_b = 2 ppm
Total Station	Leica TS60	$\sigma_{Hz,V}$ = 0.5" σ_a = 0.600 mm σ_b = 1 ppm

The laser trackers take measurements to spherically mounted retroreflectors (SMRs) that are 1.5" in diameter. AMD has developed custom survey monuments called "Kyjak bolts" (see Fig. 2) which hold SMRs securely in

place using permanent magnets. Experience has shown these Kyjak bolts to be precise and durable.

Figure 2: Pictures of Kyjak Bolt.

Control points were placed in the following way for each tunnel cross-section with typically 5 meters of spacing between cross-sections (see Fig. 3):

- 1 on the left wall approximately 1 foot off the floor
- 1 on the left wall approximately 4 feet off the floor
- 2 on the right wall in the same manner
- 1 on the floor between both walls

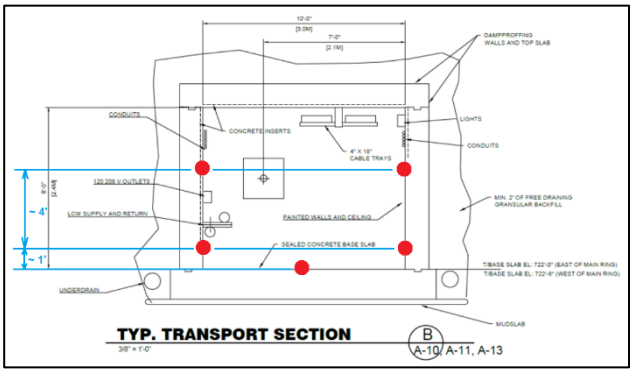

Figure 3: Typical Tunnel Control Point Placement.

Figures 1 and 4 show the placement of the control points and the instrument locations. Note that these control points are also compatible with AMD's barcode staffs that are used with the digital levels. The barcode staffs have a 1.5" spherical base that connects to the Kyjak bolt in the same manner as an SMR. Laser tracker locations were normally spaced every 15 meters in the pre-analysis, observation lines were kept to less than 15 meters in length, and every control point was measured twice by an instrument. The same instrument positions and observation lines were used for both the laser tracker and digital level (i.e. they are co-located). This was done out of convenience and the results should be comparable. Total station measurements were also included with the main purpose to strengthen the geometry with long-range horizontal angle measurements. In total, there were 621 control points, 52 laser tracker/digital level setups, 1257 laser tracker/digital level observation sets (each set contains a horizontal direction, vertical angle, slope distance, and rod reading measurement), 8 total station setups, and 56 total station observation sets (each set contains a horizontal direction, vertical angle, and slope distance measurement).

Weighted Constraints

As discussed previously, three groups of control points will be held with weighted constraints to perform the TN adjustment: sight-riser, Booster connection, and HBB. A-priori uncertainties for these three point groups needed to be chosen for the pre-analysis. The error budget involves two main contributions for the sight-riser group: the uncertainty in the surface-level point, and the error in transferring that point into the tunnel through the sight-riser. The magnitude of the first contribution was determined from a previous horizontal pre-analysis of the PIP-II SN computed by AMD [7], where the maximum horizontal uncertainty out of five sight-riser points was 0.218 mm. Regarding the second contribution, the sight-riser points will be transferred into the tunnel using a Wild NL nadir plummet which, based on previous experience, has a horizontal uncertainty of 0.250 mm for a 10-meter drop. These two errors taken in quadrature give a total horizontal uncertainty of 0.332 mm in both dimensions.

This estimate only provides a horizontal uncertainty but is missing a vertical uncertainty. In addition, there is no information that directly gives a-priori estimates for the Booster connection and HBB control points. Historical data from another network adjustment was used to fill in this missing information as the methodology was similar. The 2006 Tevatron network adjustment achieved an absolute accuracy of: $\sigma_x = 0.325$ mm, $\sigma_y = 0.315$ mm, $\sigma_z = 0.315$ mm [8].

The 2D errors from the first estimate closely agree with the 2006 Tevatron network adjustment results. Taking all of this into account, the following uncertainties were chosen for the sight-riser, Booster connection, and HBB control points: $\sigma_x = \sigma_y = \sigma_z = 0.325$ mm.

Pre-Analysis Results

An in-house least squares adjustment program was written in Python to compute the 3D uncertainties using error propagation. The mean/max uncertainty values are shown in Table 5 and the single-point error ellipse plots are shown in Fig. 4. (note that the observations have been separated into two plots to make them easier to read).

Table 5: Pre-Analysis Results

Station Uncertainties	**Hz (2D) / V(1D), mm**
Mean Absolute	0.152 / 0.055
Max Absolute	0.210 / 0.069
Mean Relative (< 100 m)	0.105 / 0.030
Max Relative (< 100 m)	0.212 / 0.067

DESIGN VERIFICATION

We can see from Table 5 that tolerance requirements (1) and (2) have been meet. Verifying tolerance requirement (3) was more involved as both global and local errors needed to be determined and taken in quadrature, and these will now both be discussed.

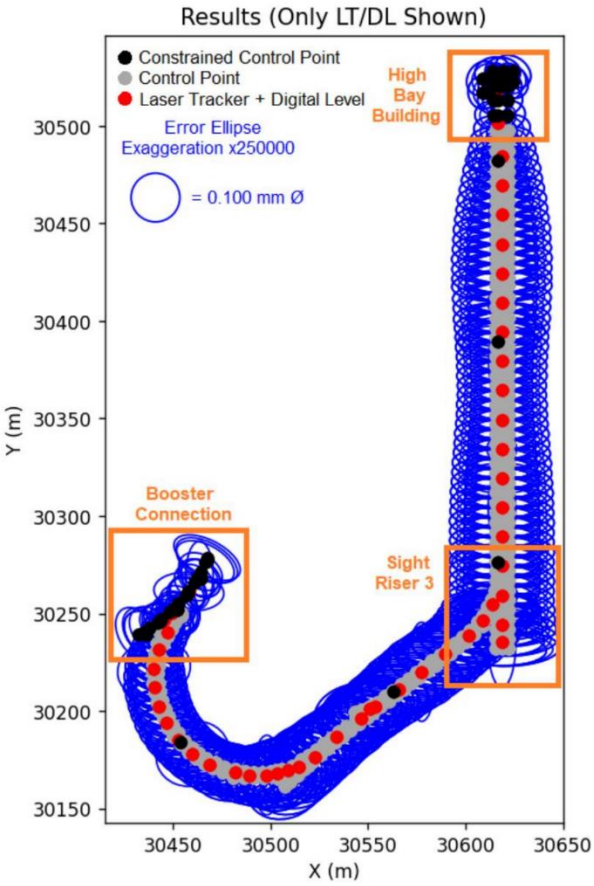

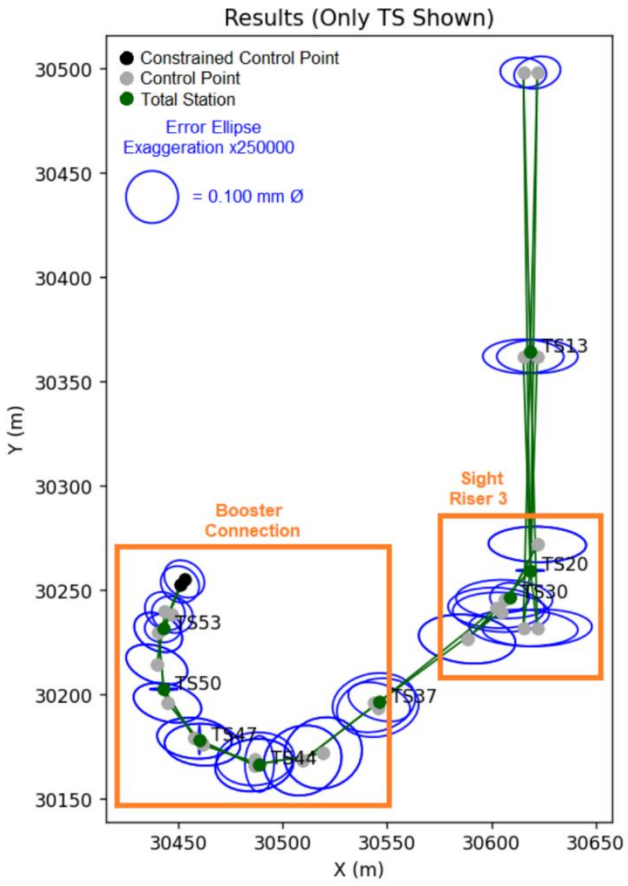

Figure 4: Tunnel Network Pre-Analysis Results.

Global Alignment Errors - Network Uncertainty

The relative uncertainties between nearby control points are usually small, but the absolute placement of the points themselves will vary throughout the tunnel, and this will correspondingly cause global errors in the position and orientation of the machine components. Fig. 5 shows this effect from an overhead view. The black points represent the recorded control point positions. The red points, however, represent the true control point positions which are unknown due to measurement errors. Although the relative geometry between the points is correct, the absolute errors show a translation in the longitudinal axis, a translation in the transverse axis, and a yaw rotation. As can be seen in Fig. 5, this corresponds to translation and rotation errors in the placement of the machine component.

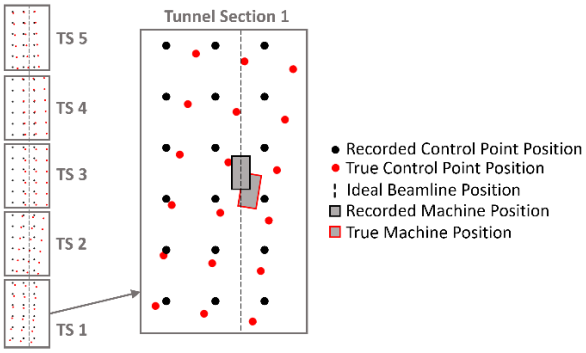

Figure 5: Network Uncertainty Diagram.

There is a difficulty in describing these absolute alignment errors because the coordinate uncertainties are positional quantities (X, Y, Z), and therefore do not describe orientation alignment errors (pitch, roll, and yaw) which are angular quantities. The proposed solution to this difficulty is to divide the tunnel into sections and to propagate the global coordinate uncertainties through 6-parameter Helmert transformations. To describe the concept, consider two point groups that contain the same common points of a tunnel section but with slightly different coordinates. The coordinates of the first point group contain errors (black points in Fig. 5) and the coordinates of the second point group are true and errorless (red points in Fig. 5). To remove the errors in the first group, the points could be shifted and rotated so that they correspond to the points in the second group. Those same shifts and rotations could then be applied to the recorded machine position/orientation (black machine in Fig. 5) to compute the true machine position/orientation (red machine in Fig. 5). A best-fit six-parameter Helmert transformation could be used to find these required shifts and rotations.

We can use the following parametric model to find the uncertainties in these shifts and rotations:

$$\vec{r}' = R\vec{r} + T$$

$$x' = R_{row1}\vec{r} + T_x$$

$$y' = R_{row2}\vec{r} + T_y$$

$$z' = R_{row3}\vec{r} + T_z$$

$$R = R(\theta_z)R(\theta_y)R(\theta_x) = R_z R_y R_x$$

where $\vec{r}'$ represents the coordinate column vector of a point in the erroneous point group, $\vec{r}$ represents the coordinate column vector of a point in the errorless point group, $T_x/T_y/T_z/\theta_x/\theta_y/\theta_z$ are the three translation and rotation parameters, respectively, R is the 3D rotation matrix, and T is the translation column vector containing $T_x/T_y/T_z$. To compute the uncertainty in the six transformation parameters:

$$A_a = \begin{bmatrix} \frac{\partial x_1'}{\partial T_x} & \frac{\partial x_1'}{\partial T_y} & \frac{\partial x_1'}{\partial T_z} & \frac{\partial x_1'}{\partial \theta_x} & \frac{\partial x_1'}{\partial \theta_y} & \frac{\partial x_1'}{\partial \theta_z} \\ \frac{\partial y_1'}{\partial T_x} & \frac{\partial y_1'}{\partial T_y} & \frac{\partial y_1'}{\partial T_z} & \frac{\partial y_1'}{\partial \theta_x} & \frac{\partial y_1'}{\partial \theta_y} & \frac{\partial y_1'}{\partial \theta_z} \\ \frac{\partial z_1'}{\partial T_x} & \frac{\partial z_1'}{\partial T_y} & \frac{\partial z_1'}{\partial T_z} & \frac{\partial z_1'}{\partial \theta_x} & \frac{\partial z_1'}{\partial \theta_y} & \frac{\partial z_1'}{\partial \theta_z} \\ & & & \vdots & & \\ \frac{\partial x_n'}{\partial T_x} & \frac{\partial x_n'}{\partial T_y} & \frac{\partial x_n'}{\partial T_z} & \frac{\partial x_n'}{\partial \theta_x} & \frac{\partial x_n'}{\partial \theta_y} & \frac{\partial x_n'}{\partial \theta_z} \\ \frac{\partial y_n'}{\partial T_x} & \frac{\partial y_n'}{\partial T_y} & \frac{\partial y_n'}{\partial T_z} & \frac{\partial y_n'}{\partial \theta_x} & \frac{\partial y_n'}{\partial \theta_y} & \frac{\partial y_n'}{\partial \theta_z} \\ \frac{\partial z_n'}{\partial T_x} & \frac{\partial z_n'}{\partial T_y} & \frac{\partial z_n'}{\partial T_z} & \frac{\partial z_n'}{\partial \theta_x} & \frac{\partial z_n'}{\partial \theta_y} & \frac{\partial z_n'}{\partial \theta_z} \end{bmatrix}$$

$$C_l' = \begin{bmatrix} \sigma_{x_1'}^2 & \sigma_{y_1'x_1'}^2 & \sigma_{z_1'x_1'}^2 & & \sigma_{x_n'x_1'}^2 & \sigma_{y_n'x_1'}^2 & \sigma_{z_n'x_1'}^2 \\ \sigma_{x_1'y_1'}^2 & \sigma_{y_1'}^2 & \sigma_{z_1'y_1'}^2 & \cdots & \sigma_{x_n'y_1'}^2 & \sigma_{y_n'y_1'}^2 & \sigma_{z_n'y_1'}^2 \\ \sigma_{x_1'z_1'}^2 & \sigma_{y_1'z_1'}^2 & \sigma_{z_1'}^2 & & \sigma_{x_n'z_1'}^2 & \sigma_{y_n'z_1'}^2 & \sigma_{z_n'z_1'}^2 \\ & \vdots & & \ddots & & \vdots & \\ \sigma_{x_1'x_n'}^2 & \sigma_{y_1'x_n'}^2 & \sigma_{z_1'x_n'}^2 & & \sigma_{x_n'}^2 & \sigma_{y_n'x_n'}^2 & \sigma_{z_n'x_n'}^2 \\ \sigma_{x_1'y_n'}^2 & \sigma_{y_1'y_n'}^2 & \sigma_{z_1'y_n'}^2 & \cdots & \sigma_{x_n'y_n'}^2 & \sigma_{y_n'}^2 & \sigma_{z_n'y_n'}^2 \\ \sigma_{x_1'z_n'}^2 & \sigma_{y_1'z_n'}^2 & \sigma_{z_1'z_n'}^2 & & \sigma_{x_n'z_n'}^2 & \sigma_{y_n'z_n'}^2 & \sigma_{z_n'}^2 \end{bmatrix}$$

$$C = (A_a^T C_l'^{-1} A_a)^{-1}$$

where $(x_1', y_1', z_1', \ldots, x_n', y_n', z_n')$ is the subgroup of points that are contained in each tunnel section, A_a is the design matrix that linearizes the parametric model to first order, C_l' is the variance-covariance (VCV) sub-matrix of the global coordinate uncertainties obtained earlier from the pre-analysis, and C is the resulting VCV matrix of the six transformation parameters. Note that the sub-matrix C_l' is built by selecting only the elements from the main VCV matrix that correspond to the points contained in each tunnel section.

The length of each tunnel section was set to be the same as the typical operating range of the laser tracker and digital level in the tunnel environment (typically 12.5 meters in each direction which equals 25-meter tunnel sections). It was therefore decided to use the 52 laser tracker/digital level instrument positions already established in the pre-analysis to delineate the tunnel sections. The maximum uncertainties are shown in Table 6. Note that there is a separate row for the warm front end because of the more stringent tolerance requirements, namely the 200 Ohm kicker.

Local Alignment Errors

The focus of the local analysis was modelling the errors based on standard metrology procedures. To be most realistic, the uncertainties of measuring the fiducial markers as well as measuring individual electrical and mechanical features (i.e., electrical centers via stretch-wire, alignment centerline of the strongback using the endcaps, alignment centerline of the vacuum vessel using the flange centers, stud positions, etc.) would need to be included. However, it was decided to limit the analysis to the fiducial markers only due to time constraints. Although this should still provide a reasonable error estimate, future work should include these other error sources for a more realistic estimate.

A separate local error analysis was performed for the warm and cold beamline components because there is a significant difference in the uncertainty between the two (see Fig. 6). In the former, the components are installed on girder rails and are accessible in their final locations which allows them to be directly aligned in the tunnel. In the latter, the components are not accessible because they are first inserted into the vacuum vessel. There is a much larger uncertainty because of all the additional required steps, primarily: the alignment of each component relative to the strongback, the insertion of the component-string/strongback into the vacuum vessel, and the placement of the vacuum vessel inside the tunnel.

The local error analysis was broken down into two major segments for both warm and cold beamline components: stand adjustment and measurement noise. These two segments will now be discussed.

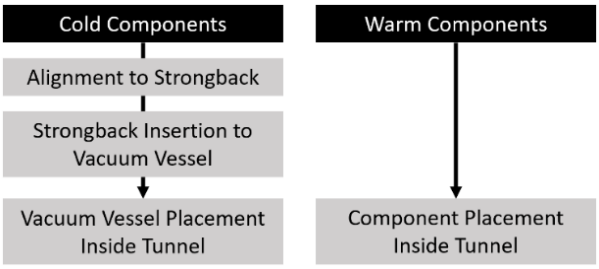

Figure 6: Error Stack-Up of Cold vs. Warm Components.

Stand Adjustment Errors A component is normally attached to an adjustment stand that keeps the component secured in place and allows for its position and orientation to be adjusted by some method such as turning finely threaded bolts or studs. There are limits on how precise these adjustments can be made because of mechanical limitations. For example, tightening down the bolts to secure the component in its final position may undesirably cause

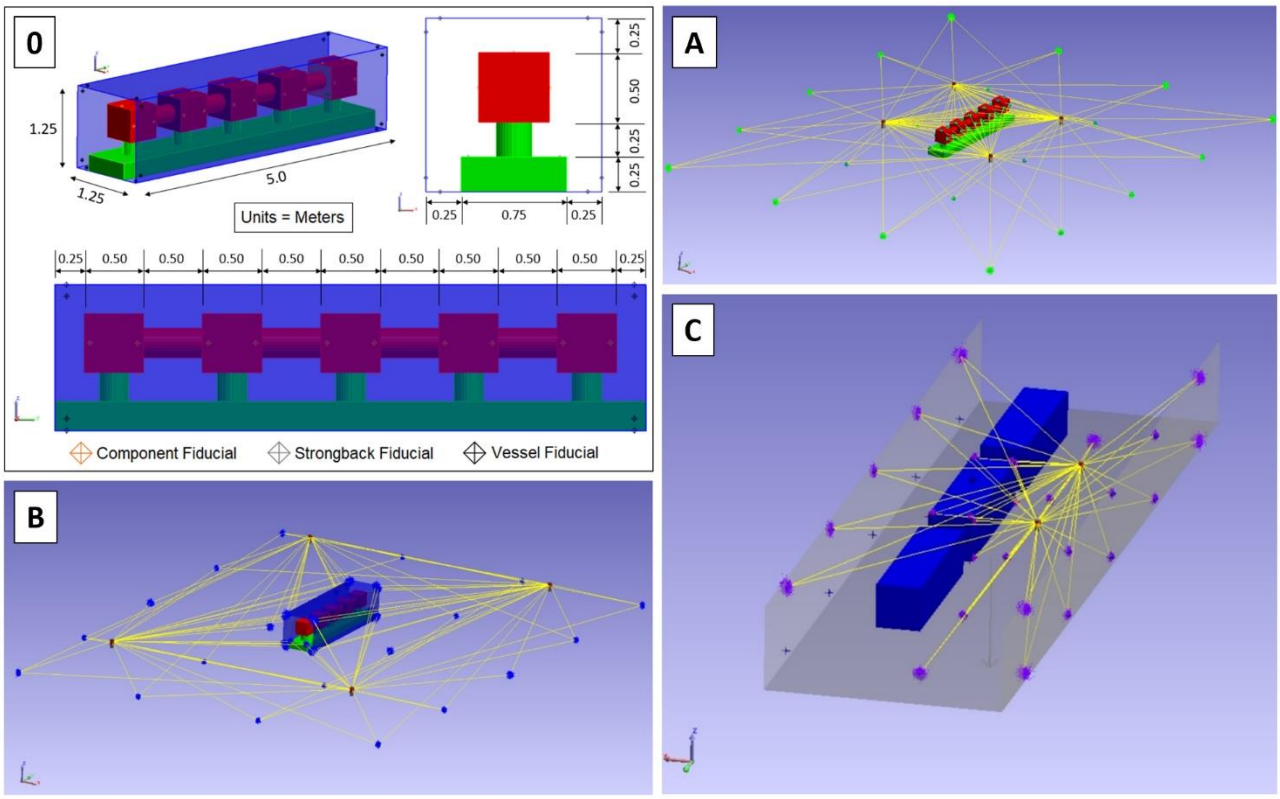

Figure 7: [0] Simulation Assembly Model, [A] Component Alignment to Strongback, [B] Cavity String/Strongback Insertion to Vacuum Vessel, [C] Placement of Vacuum Vessel Inside Tunnel.

the component to slightly move once a large enough torque is applied.

There is a certain level of precision that is normally achievable in positioning each component fiducial without spending a very large amount of time. AMD has found with experience that setting each fiducial to less than 0.100 mm strikes a balance between precision and practicality. The magnitude of this tolerance is significant enough that its effect on the final component uncertainties was considered.

A Monte Carlo approach was used in Python to simulate stand adjustment errors. Random shift (transverse, vertical, longitudinal) and orientation (pitch, yaw, roll) errors were generated using a uniform probability distribution. The misalignment errors would be accepted if all measured fiducials on the component/strongback/vessel were within 0.100 mm of their ideal positions. Otherwise, new shift and orientation errors would be generated, and the fiducials would be checked again. A total of 1000 simulations were run for both warm and cold beamline components.

Measurement Noise The software "SpatialAnalyzer" (New River Kinematics, Virginia, USA) was used to compute the measurement noise for the local errors using the "Uncertainty Field Analysis" feature.

Cold Component Errors The most realistic analysis would involve using a separate model of every single component and assembly (LEBT, MEBT, HWR, HB650, etc.). Due to time constraints, however, only one single model was used that was a reasonable approximation of all the components and assemblies. The chosen assembly model is shown in Fig. 7 and the measurement process is described below:

A. Five components (0.5m x 0.5m x 0.5m) are aligned to the strongback (0.75m x 0.25m x 5.0m).
B. The strongback, along with the 5 aligned components, is inserted and aligned to the vacuum vessel (1.25m x 1.25m x 5.0m).
C. The vacuum vessel is placed in the tunnel in its final position.

A stand adjustment pre-analysis was performed for (A) – (C) as previously described. Unique misalignments were generated for each individual component, the strongback, and the vessel.

Transformation uncertainties were also considered in addition to instrument uncertainties for the measurement noise analysis. In practice, the component fiducials from (A) will need to be transformed into the vessel system using the strongback fiducials as common points. Then, the component fiducials will need to be transformed into the tunnel system using the vessel fiducials as common points. The custom Python program took the uncertainties from (A) – (C) and incorporated the additional transformation uncertainties. Six-parameter Helmert transformations were used to find these uncertainties. However, the mathematical model is different to the one used for the global alignment errors because there are now uncertainties in both point groups. The points in the first point group are now treated as weighted parameters to account for this:

Table 6: Verification Results (Quadrature Calculation)

Error	Transverse (mm)	Vertical (mm)	Longitudinal (mm)	Pitch (mrad)	Yaw (mrad)	Roll (mrad)
Cold Components						
Global - Network	0.201	0.057	0.168	0.008	0.009	0.004
Local - Stand	0.103	0.080	0.085	0.138	0.141	0.145
Local - Noise	0.006	0.007	0.005	0.009	0.009	0.008
Total	0.226	0.098	0.188	0.139	0.142	0.145
Warm Components						
Global - Network	0.201	0.057	0.168	0.008	0.009	0.004
Local - Stand	0.050	0.055	0.042	0.133	0.148	0.117
Local - Noise	0.006	0.007	0.005	0.009	0.009	0.008
Total	0.207	0.080	0.173	0.134	0.149	0.117
Warm – Front End						
Global - Network	0.078	0.048	0.056	0.001	0.004	0.001
Local - Stand	0.050	0.055	0.042	0.133	0.148	0.117
Local - Noise	0.006	0.007	0.005	0.009	0.009	0.008
Total	0.093	0.073	0.070	0.133	0.148	0.117

$$A_b = \begin{bmatrix} \frac{\partial x_1'}{\partial x_1} & \frac{\partial x_1'}{\partial y_1} & \frac{\partial x_1'}{\partial z_1} & & \frac{\partial x_1'}{\partial x_n} & \frac{\partial x_1'}{\partial y_n} & \frac{\partial x_1'}{\partial z_n} \\ \frac{\partial y_1'}{\partial x_1} & \frac{\partial y_1'}{\partial y_1} & \frac{\partial y_1'}{\partial z_1} & \cdots & \frac{\partial y_1'}{\partial x_n} & \frac{\partial y_1'}{\partial y_n} & \frac{\partial y_1'}{\partial z_n} \\ \frac{\partial z_1'}{\partial x_1} & \frac{\partial z_1'}{\partial y_1} & \frac{\partial z_1'}{\partial z_1} & & \frac{\partial z_1'}{\partial x_n} & \frac{\partial z_1'}{\partial y_n} & \frac{\partial z_1'}{\partial z_n} \\ & \vdots & & \ddots & & \vdots & \\ \frac{\partial x_n'}{\partial x_1} & \frac{\partial x_n'}{\partial y_1} & \frac{\partial x_n'}{\partial z_1} & & \frac{\partial x_n'}{\partial x_n} & \frac{\partial x_n'}{\partial y_n} & \frac{\partial x_n'}{\partial z_n} \\ \frac{\partial y_n'}{\partial x_1} & \frac{\partial y_n'}{\partial y_1} & \frac{\partial y_n'}{\partial z_1} & \cdots & \frac{\partial y_n'}{\partial x_n} & \frac{\partial y_n'}{\partial y_n} & \frac{\partial y_n'}{\partial z_n} \\ \frac{\partial z_n'}{\partial x_1} & \frac{\partial z_n'}{\partial y_1} & \frac{\partial z_n'}{\partial z_1} & & \frac{\partial z_n'}{\partial x_n} & \frac{\partial z_n'}{\partial y_n} & \frac{\partial z_n'}{\partial z_n} \end{bmatrix}$$

$$A = [A_a \quad A_b]$$

$$C_l' = diag\left(\sigma_{x_1'}^2 \quad \sigma_{y_1'}^2 \quad \sigma_{z_1'}^2 \quad \cdots \quad \sigma_{x_n'}^2 \quad \sigma_{y_n'}^2 \quad \sigma_{z_n'}^2\right)$$

$$C_l = diag\left(\sigma_{x_1}^2 \quad \sigma_{y_1}^2 \quad \sigma_{z_1}^2 \quad \cdots \quad \sigma_{x_n}^2 \quad \sigma_{y_n}^2 \quad \sigma_{z_n}^2\right)$$

$$C = (A^T C_l'^{-1} A + C_l^{-1})^{-1}$$

where, in addition to A_a, the design matrix A has extra columns A_b that account for the coordinates in the first point group in the form of weighted parameters, and C_l is the VCV matrix of the weighted parameters. Note that the full VCV matrix is not obtainable using SpatialAnalyzer's uncertainty estimation function, and so only diagonal elements were included in the $C_l^{'}$ and C_l matrices.

As a final step, an ideal reference was fit to the 8 fiducials on each component to estimate the uncertainty of the upstream and downstream component centers as well as the pitch, roll, and yaw uncertainties. The computed measurement noise uncertainties were found to be very small (see Table 6).

Warm Component Errors The process is much more straightforward for the warm components since they are directly placed in the tunnel on the girder rails. For the stand adjustment errors, Monte Carlo simulations were done in the same fashion previously described on a single 0.5m x 0.5m x 0.5m component only. The cold measurement noise results from the previous section already showed that the noise contribution is very small. The noise would be even smaller for the warm components and so, for convenience, the noise results from the cold analysis was used.

Verification Results

The global and local errors were added in quadrature and are shown in Table 6. Comparing against Tables 1 – 3 shows that all alignment tolerances were met except for the 200 Ohm Kicker. The vertical tolerance requirement is 0.050 mm, but the achievable value is 0.073 mm. The accelerator operators would be able to measure and provide differential shift corrections based on the generated beam if there were any beam-production issues. AMD has instruments such as micrometers and interferometers that would make possible a differential shift to an accuracy of < 0.050 mm.

CONCLUSION

A pre-analysis was performed on the proposed tunnel geodetic control network for the PIP-II construction project. The pre-analysis results were verified against the project-specific alignment tolerances using a methodology that accounted for local warm and cold component errors with a focus on the stand adjustment error and local measurement noise. The uncertainties from the tunnel network and stand adjustment error were the most significant, while the local measurement noise was negligible.

The station absolute accuracy requirement from (1) and relative station accuracy requirement from (2) were both achieved. Regarding (3), all tolerance requirements in Tables 1 – 3 were met except for the 200 Ohm Kicker (vertical: 0.073 mm > 0.050 mm). Misalignments of this component can be measured by beam-based methods in the case of beam-production issues, and differential corrections can be applied using precise instruments such as micrometers and interferometers.

Due to time constraints, the local network design verification used only a single model for all components and assemblies, and only the measurement noise and stand adjustment errors were considered. Although this should still provide a reasonable error estimate for the purposes of this project, detailed models of each component and assembly would give a more realistic estimate, and future work should also include other metrology errors (i.e., measuring electrical centers, flange centers, etc.) for the same reason.

ACKNOWLEDGEMENTS

The author would like to sincerely thank the following people for their assistance in this project:

- Technical Review – Dr. Virgil Bocean, John Kyle, Georg Gassner (SLAC National Accelerator Laboratory)
- Technical Feedback – Charles Wilson, Curtis Baffes
- Surface Network Pre-Analysis – John Kyle, Jana Barker (formerly Fermilab, now DESY)

REFERENCES

[1] Fermilab, https://pip2.fnal.gov/how-it-works/introduction/.

[2] C. Baffes *et. al.*, "PIP-II Alignment Network Technical Requirements Specification," Fermi National Accelerator Laboratory, Batavia, IL, USA, Oct. 2019.

[3] A. Saini *et. al.*, "PIP-II Misalignment Tolerances Physics Requirement Document (PRD)," Fermi National Accelerator Laboratory, Batavia, IL, USA, Nov. 2019.

[4] B. Oshinowo, "Fermilab Coordinate Systems," Fermi National Accelerator Laboratory, Batavia, IL, USA, May 1997.

[5] M. Jones, "Lattice Program Documentation," University College London, London, England, n.d.

[6] J.-P. Carneiro and E. Podzeyev, "Beam Dynamics Studies of Misalignments and RF Errors for PIP-II," Fermi National Accelerator Laboratory, Batavia, IL, USA, Feb. 2020.

[7] J. Kyle and J. Barker, "PIP-II Surface Network Pre-Analysis," Fermi National Accelerator Laboratory, unpublished.

[8] J. A. Greenwood and G. Wojcik, "Massive Metrology: Development and Implementation of a 3D Reference Frame for the Realignment of Fermilab's Tevatron," in *9th International Workshop on Accelerator Alignment (IWAA 2006)*, Stanford, CA, USA, Sep. 2006.